



A calibration framework for the determination of accurate collision cross sections of polyanions using polyoxometalate standards

S. Hupin, Hélène Lavanant, S. Renaudineau, A. Proust, G. Izzet, M. Groessl,
Carlos Afonso

► To cite this version:

S. Hupin, Hélène Lavanant, S. Renaudineau, A. Proust, G. Izzet, et al.. A calibration framework for the determination of accurate collision cross sections of polyanions using polyoxometalate standards. *Rapid Communications in Mass Spectrometry*, 2018, 32 (19), pp.1703-1710. 10.1002/rcm.8230 . hal-02024506

HAL Id: hal-02024506

<https://normandie-univ.hal.science/hal-02024506>

Submitted on 3 Jun 2024

HAL is a multi-disciplinary open access archive for the deposit and dissemination of scientific research documents, whether they are published or not. The documents may come from teaching and research institutions in France or abroad, or from public or private research centers.

L'archive ouverte pluridisciplinaire **HAL**, est destinée au dépôt et à la diffusion de documents scientifiques de niveau recherche, publiés ou non, émanant des établissements d'enseignement et de recherche français ou étrangers, des laboratoires publics ou privés.



Distributed under a Creative Commons Attribution - NonCommercial - NoDerivatives 4.0 International License

**A calibration framework for the determination of accurate collision cross
sections of polyanions using polyoxometalate standards**

Sébastien Hupin[†], Hélène Lavanant^{*,†}, Séverine Renaudineau[‡], Anna Proust[‡], Guillaume Izzet[‡], Michael Groessl[§], Carlos Afonso[†]

[†] Normandie Univ, UNIROUEN, INSA Rouen, CNRS, COBRA, 76000 Rouen, France

[‡] Sorbonne Universités, UPMC Univ Paris 06, CNRS UMR 8232, Institut Parisien de Chimie Moléculaire, 4 Place Jussieu, F-75005 Paris, France

[§] Department of Nephrology and Hypertension and Department of BioMedical Research, Inselspital, Bern University Hospital, University of Bern, Switzerland

* Corresponding author

Université de Rouen,
IRCOF, 1 Rue Tesnière,
76821 Mont-Saint-Aignan Cedex, France
Tel: +33 2 35 52 29 32
Helene.lavanant@univ-rouen.fr.

RATIONALE:

Polyoxometalates (POM) are remarkable oxo-clusters forming compact highly charged anions. We measured their collision cross sections (CCS) in N₂ with drift tube ion mobility spectrometry (DTIMS). These values were then used to calibrate a traveling wave ion mobility spectrometry (TWIMS) device and the accuracy of the calibration was tested.

METHODS:

Six POM standards were analyzed by DTIM-MS (Tofwerk, Thun, Switzerland) at different voltages to determine absolute ^{DT}CCS(N₂). Five POM compounds (Lindqvist TBA₂Mo₆O₁₉; decatungstate TBA₄W₁₀O₃₂; Keggin TBA₃PMo₁₂O₄₀; TBA₃PW₁₂O₄₀ and Dawson TBA₆P₂W₁₈O₆₂) were used for the calibration of TWIM-MS instrument (Synapt G2 HDMS, Waters, Manchester) and a sixth Dawson POM, TBA₉P₂Nb₃W₁₅O₆₂, was used to compare the accuracy of the calibrations with POM or with polyalanine and dextran reference ions.

RESULTS:

We determined forty-five ^{DT}CCS(N₂) values at 30°C or 60°C. Fourteen ^{DT}CCS(N₂) values at 30°C were used to perform calibration of the TWIMS. Better correlations were observed than when ^{DT}CCS values in helium from the literature were used.

The accuracy tests on six ions of Dawson POM TBA₉P₂Nb₃W₁₅O₆₂ led to relative errors below 3% while relative errors of 4.1% to 10.1% were observed when calibration was performed with polyalanine and dextran reference ions.

CONCLUSIONS:

Our novel calibration strategy for determination of CCS values of multiply negatively charged ions on TWIM-MS devices based on ^{DT}CCS(N₂) of standard POM structures covered a wider range of CCS and improved the accuracy to 2% relative error on average compared to 7.5% using polyalanine and dextran calibration.

INTRODUCTION

Polyoxometalates are an interesting class of oxo-clusters with an incomparable diversity of structures, properties, and potentials applications.^{1,2} POMs are constituted of multiple polyhedra {MO_x} sharing O atoms, (where M is a group 5 or 6 transition metal such as Mo^{VI} or W^{VI}) and form compact and highly negative charged structures.³

Since the earlier reports of POM analysis by mass spectrometry (MS) with electrospray ionization (ESI) in 1995,⁴ ESI-MS has proven to be a powerful tool for the analysis of POM compounds,^{5,6} and particularly for characterizing large POM-based assemblies.^{7–9}

The coupling of ion mobility spectrometry (IMS) to mass spectrometry has more recently provided a new separation dimension for the analysis of complex mixtures or multimeric species.^{10,11} Ion mobility-mass spectrometry (IM-MS) is growing into a new analytical technique that applies to many areas of chemical and biological research.¹² In classic drift-tube IMS (DTIMS), ions are accelerated by a uniform electric field, and the reduced mobility (K_0), which is intrinsic to the ion and the buffer gas density, is generally reported (equation 1).^{13–15}

$$K_0 = K \times \frac{273.2}{T} \times \frac{P}{760} = \frac{L}{t_D E} \times \frac{273.2}{T} \times \frac{P}{760} \quad (1)$$

where K is the ion mobility (in m² s⁻¹ V⁻¹), L is the drift tube length (in m), t_D is the drift time (in s), E is the applied electric field (in V m⁻¹), T is the temperature (in K) and P is the pressure (in Torr).

With conventional IMS, where the electric field is a uniform field, it is possible to calculate the collision cross section (CCS) of the ion based on its ion mobility, using the Mason-Schamp equation (equation 2):¹⁴

$$\Omega = \frac{(18\pi)^{\frac{1}{2}}}{16} \frac{ze}{(k_B T)^{\frac{1}{2}}} \left(\frac{1}{\mu}\right)^{\frac{1}{2}} \frac{1}{N} \frac{1}{K} \quad (2)$$

where N is the number density of the buffer gas, ze is the ion charge, k_B is the Boltzmann constant, T is the temperature (in K), μ is the reduced mass of the analyte and the drift gas and Ω is the cross collision section.

The CCS accounts for the repeated binary collisions that take place between the ion and the neutral buffer gas molecules in the mobility cell, orientally averaging all possible ion-neutral collisions over scattering angles and collision energies; it depends largely on the conformation of the ion, its charge and, as it is a two-body process, the buffer gas chosen.

Other IM techniques, such as traveling wave ion mobility spectrometry (TWIMS), where the electric field is not uniform, can also be coupled to the MS. In these techniques, a CCS estimation requires calibration with compounds with known CCS values. These reference values are generally obtained from measurements with drift tube ion mobility spectrometers using helium (^{DT}CCS(He)) or nitrogen (^{DT}CCS(N₂)) as drift gas. Many such ^{DT}CCS values are

available in positive and negative ion mode and are listed in locally curated databases, such as the Clemmer,^{15–22} Bush^{23–26} or the McLean²⁷ CCS databases.

In the negative ionization mode, still few reference values exist until now : compounds of known ^{DT}CCS(He) or ^{DT}CCS(N₂) values include poly-DL-alanine,²⁸ polymalic acid,²⁸ polystyrene,²⁹ dextran³⁰ or phosphoric acid cluster ions.³¹ In the case of polystyrene and phosphoric acid cluster ions, only ^{TW}CCS or calculated CCS are available. The standards proposed in negative mode with known ^{DT}CCS(N₂) are all singly charged species with large CCS values, unlike POM which are compact and multiply-charged. The few reported multiply charged ^{DT}CCS(He) values^{17,20} are all based on oligonucleotides and deprotonated proteins.

For TWIMS calibration, Smith *et al.*³² have described a method using a reduced collision cross section (Ω') (equation 3), which is the part of the ion mobility that depends on the molecules (including the charge z and reduced mass μ) and not the experimental parameters (temperature T and number density N). The method uses a correlation between this reduced collision cross section Ω' and the drift time using a power function (equation 4).

$$\Omega' = \frac{\sqrt{\mu}}{z} \Omega \quad (3)$$

$$\Omega' = At_D^B \quad (4)$$

In equation 4, A may be viewed as a correction factor for temperature and pressure and B as a compensation for the non-linear effect of the TWIMS device.

In our case, we have linearized this equation by using natural logarithms, in order to have a linear regression. The correlation obtained from standards of known ^{DT}CCS and their drift time measured using the TWIMS cell may then be used to estimate the collision cross section, termed ^{TW}CCS, for others compounds. As the TWIMS device is always operated with N₂ buffer gas, these ^{TW}CCS values will be noted ^{TW}CCS(N₂→N₂) or ^{TW}CCS(N₂→He) depending on whether ^{DT}CCS(N₂) or ^{DT}CCS(He) were used to obtain the correlation.

Some recent ion mobility studies have been carried out on POMs. Indeed, Thiel *et al.* observed in 2011 the self-assembly of a hybrid POM by TWIM-MS.³³ Izzet *et al.* in 2015 showed the formation of POM self-assembling in the presence of palladium with a TWIM-MS device, and did ^{TW}CCS(N₂→He) estimations, using cytochrome *c* and olygothymidine dT₁₀ as calibrant ions.³⁴

A few POM ^{DT}CCS in helium have been reported by Surman *et al.* in 2016.³⁵ They have measured ^{DT}CCS(He) for four POM structures : two Mn-Anderson clusters (C₁₆H₃₆N)₃[MnMo₆O₂₄(C₄H₈N)₂] and (C₁₆H₃₆N)₃[MnMo₆O₂₄(C₂₀H₃₈NO)₂], a Keggin POM (C₁₆H₃₆N)₃[PW₁₂O₄₀]) and a Dawson POM (C₁₆H₃₆N)₆[P₂W₁₈O₆₂]). We wanted to complete these existing reference values in helium by ^{DT}CCS measurements in nitrogen for this class of oxo-clusters compounds.

In this paper, we present the measurement of a set of forty-five ${}^{DT}CCS(N_2)$ values obtained from a series of standards isopolyoxometalates (Lindqvist structure $TBA_2Mo_6O_{19}$, and decatungstate $TBA_4W_{10}O_{32}$), and heteropolyoxometalates (Keggin structures $TBA_3PMo_{12}O_{40}$ and $TBA_3PW_{12}O_{40}$), and Dawson structures ($TBA_6P_2W_{18}O_{62}$ and $TBA_9P_2Nb_3W_{15}O_{62}$) at two different temperature (30°C and 60°C). Seven of these ${}^{DT}CCS(N_2)$ values at 30°C were compared to the ${}^{DT}CCS(He)$ measured by Surnam *et al.*³⁵

We then used fourteen of our ${}^{DT}CCS(N_2)$ values at 30°C to calibrate the TWIMS cell and compared the correlation with the correlations obtained from reference compounds polyalanine, dextran and dT_{10} and their ${}^{DT}CCS(He)$ or ${}^{DT}CCS(N_2)$ values. Finally, we studied how the differences in calibration affected the accuracy of ${}^{TW}CCS$ estimations on Dawson structure POM compound $TBA_9P_2Nb_3W_{15}O_{62}$.

METHODS

Materials

The six polyoxometalates as tetrabutylammonium (TBA) salts ($TBA_2Mo_6O_{19}$;³⁶ $TBA_4W_{10}O_{32}$;³⁶ $TBA_3PMo_{12}O_{40}$;³⁶ $TBA_3PW_{12}O_{40}$;³⁷ $TBA_6P_2W_{18}O_{62}$;³⁸ $TBA_9P_2Nb_3W_{15}O_{62}$;³⁹) were synthesized at the IPCM (Paris, France) using reported synthetic procedures. HPLC grade acetonitrile were purchased from Fisher Chemical (Illkirch, France). Deionized water (18 MΩ) was obtained from a milli-Q apparatus (Millipore, Bedford, MA, USA).

Poly-DL-alanine, dextran, dT_{10} oligonucleotide were all provided by Sigma-Aldrich (St Louis, USA). The six tetrabutylammonium polyoxometalates were dissolved separately in pure acetonitrile to a concentration of 10^{-5} M. A solution with the six mixed POMs was also prepared in pure acetonitrile at the same concentration of 10^{-5} M.

Drift tube ion mobility

All drift tube ion mobility-mass spectrometry (DTIM-MS) measurements were carried out on a Tofwerk IMS-TOF (Thun, Switzerland), equipped with an ESI source, a 10 cm desolvatation tube and a 20.555 cm drift tube, as described in detail elsewhere.⁴⁰ The temperature of desolvatation tube and drift tube was regulated at 30.0°C and 30.7°C respectively. Nitrogen was used as the buffer gas with a pressure of 1000 mbar. Ion mobility was carried out at five different field strengths between 300 and 450 V cm⁻¹ (reduced electric field E/N *ca.* 1-2 Td). Samples were introduced directly into the ESI source at 1 μ l min⁻¹. The instrument was operated from *m/z* 50 to 1700 in negative ion mode with a measurement time of 2 to 5 min at each field strength. The mass spectrometer was calibrated internally.

Raw IMS-TOF data was post-processed using Tofware 2.5.6 software (Tofwerk, Switzerland). The ion mobility values K are determined from a plot of the measured drift time vs the inverse drift voltage at five different voltages (potentials from 8 to 12 kV). Reduced mobilities K_0 and collision cross sections, noted ${}^{DT}CCS(N_2)$, can then be directly calculated from the slopes of the drift time vs the inverse drift voltage and using the Mason-Schamp equation.¹⁴

Traveling wave ion mobility

Traveling wave ion mobility TWIM-MS experiments were carried out by using a Synapt G2 HDMS (Waters Corp, Manchester, UK) instrument equipped with an ESI source. The solution was infused at a flow rate of $3 \mu\text{L min}^{-1}$ using a syringe-pump. ESI mass spectra were acquired over the m/z 50-5000 range in the negative-ion mode with a capillary high voltage of 2.0 kV and sampling cone of 10 V. The source temperature was set at 90 °C. Nitrogen gas at a temperature of 250 °C and a flow rate of 500 L h⁻¹ was used to assist desolvation in the ESI source. All desolvation, transmission ion mobility parameters were tuned to limit gas-phase ion fragmentation. The traveling wave ion mobility spectrometry cell that was operated with N₂ as the buffer gas. Gas flow rates were set at 20 mL min⁻¹ in the source stacked ring ion guide, 180 mL min⁻¹ in the helium cell and 70 mL min⁻¹ in the ion mobility cell. Trap and transfer collision energies were set to 4 and 0 V, respectively. IMS parameters were as follows: source wave and trap velocities at 300 m s⁻¹ with a wave height at 0.2 V and 5.0 V respectively, and IMS wave and transfer wave velocities at 350 m s⁻¹ with a wave height at 15.0 V and 5.0 V respectively.

Data treatment was carried out with MassLynx software V.4.1 and DriftScope software V.2.2 (Waters, Manchester). All TWIMS spectra were fitted to Gaussian curves with OriginPro 8.5 (OriginLab) to obtain experimental drift times with maximum accuracy.

RESULTS AND DISCUSSION

POM mass spectra

POM standards have been chosen to cover a range of different masses, structures and charges states. They have the particularity to be very stable in solution.

Figure 1 shows the four types of structures chosen for POM standards, all isolated as tetrabutylammonium (TBA) salts. Among these, we used a Lindqvist structure, TBA₂Mo₆O₁₉, a decatungstate TBA₄W₁₀O₃₂ structure, two Keggin structures TBA₃PMo₁₂O₄₀ and TBA₃PW₁₂O₄₀ and two Dawson structures TBA₆P₂W₁₈O₆₂ and TBA₉P₂Nb₃W₁₅O₆₂.

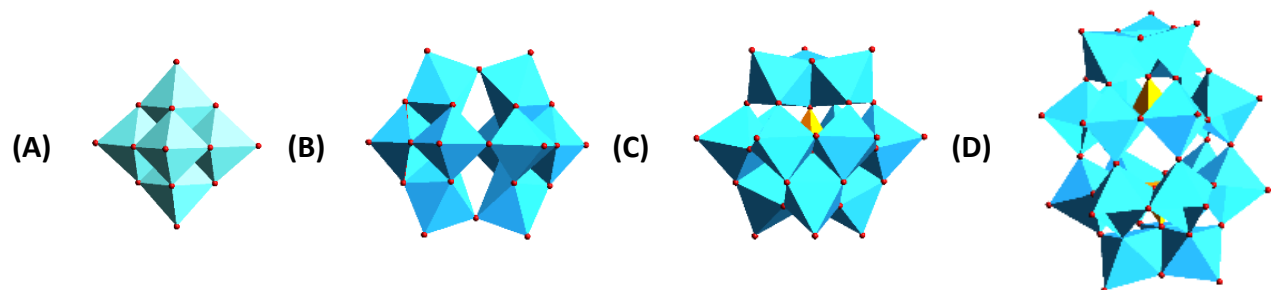


Figure 1: Representations of the four POM structures calibrants in this study. Metal oxide units represented as polyhedra with metal atoms inside and oxygen atoms outside. (A) Lindqvist structure (B) Decatungstate Structure (C) Keggin structure (D) Dawson structure.

The mass spectra of the six POM compounds under electrospray ionization displayed signals from the POM anions associated with TBA⁺ counter-ions and also “naked” POM anions, without any TBA counterions.

Figure 2 shows the ESI-MS mass spectrum of TBA₃PW₁₂O₄₀. Two main isotopic distribution can be observed at m/z 959 and m/z 1560, corresponding to [PW₁₂O₄₀]³⁻ and [PW₁₂O₄₀+TBA]²⁻

respectively, and overlapping to the theoretical isotopic distribution (dark grey). Additional mass spectra of POMs are given in supplementary information.

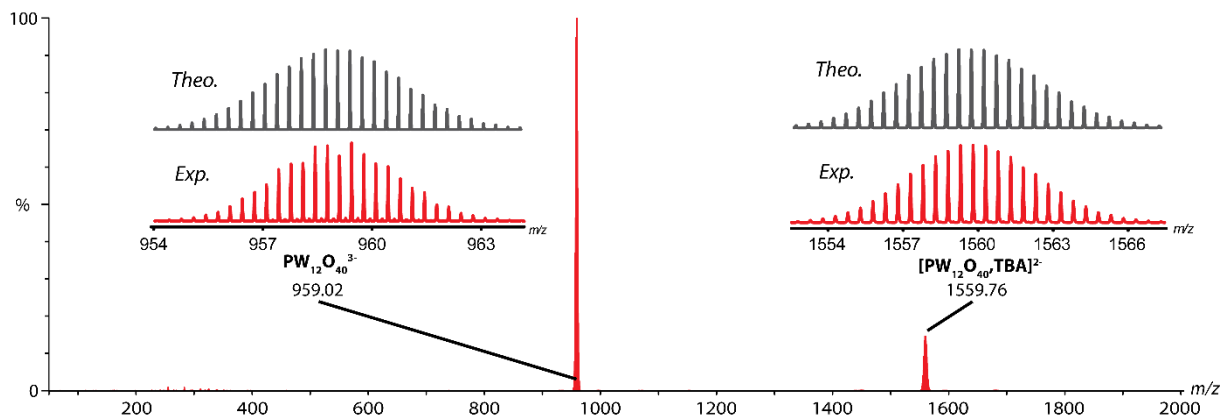


Figure 2: ESI-MS of $\text{TBA}_3\text{PW}_{12}\text{O}_{40}$ ($10\mu\text{M}$) in acetonitrile. The main ion distributions correspond to the “naked” POM $[\text{PW}_{12}\text{O}_{40}]^{3-}$ (m/z 959) and the POM with counter ion $[\text{PW}_{12}\text{O}_{40}+\text{TBA}]^{2-}$ (m/z 1560). Inset: Comparison of experimental (lower trace) and calculated (upper trace) isotopic distributions for m/z 959 and 1560.

Several clusters with H^+ counter-ions were also observed on the mass spectra of three POM ($\text{TBA}_4\text{W}_{10}\text{O}_{32}$ and the two Dawson structures $\text{TBA}_6\text{P}_2\text{W}_{18}\text{O}_{62}$ and $\text{TBA}_9\text{P}_2\text{Nb}_3\text{W}_{15}\text{O}_{62}$) (table 1 and SI) resulting in the formation of clusters $[\text{POM} + x\text{TBA} + y\text{H}]^{[n-(x+y)]-}$, where n is the POM naked charge, x the number of TBA^+ counter ions and y the number of H^+ (proton). The presence of H^+ in an aprotic and polar solvent as acetonitrile was surprising and may arise from the loss of neutral fragments from TBA^+ , but such fragmentation could not be observed in MS/MS spectrum. Residual water in the solvent or the atmospheric source could also be responsible.

DTIMS CCS determination in nitrogen

The drift times of each POM ion were measured at five different voltages. For example, Figure 3(A) shows the drift times of the $[\text{PW}_{12}\text{O}_{40} + \text{TBA}]^{2-}$ (m/z 1559) ion at 8 kV, 9 kV, 10 kV, 11 kV and 12 kV voltages.

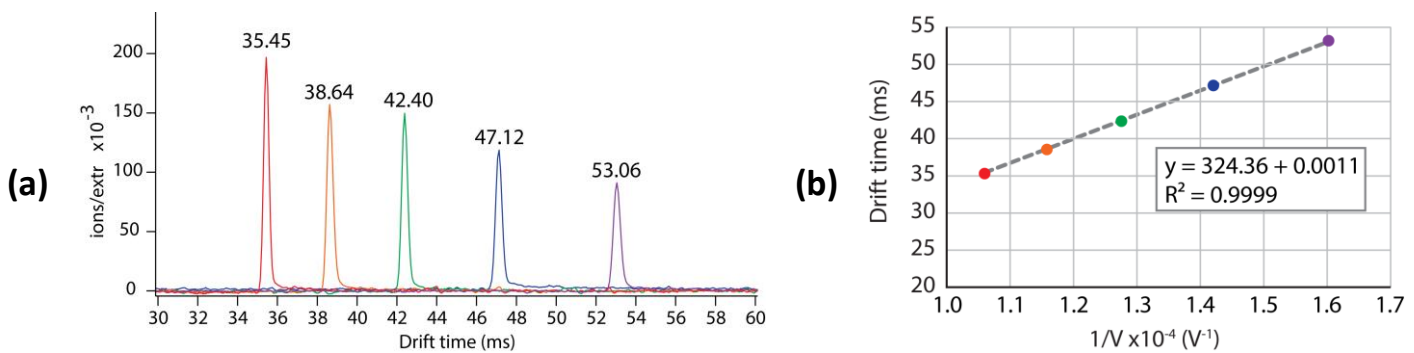


Figure 3 : (a) DTIMS spectra of $[\text{PW}_{12}\text{O}_{40} + \text{TBA}]^{2-}$ ion (m/z 1559) at different voltages. Red: 12 kV, orange: 11 kV, green: 10 kV, blue: 9 kV and purple: 8 kV. (b) Drift time vs $1/V$ plots of $[\text{PW}_{12}\text{O}_{40} + \text{TBA}]^{2-}$ ion (m/z 1559). Color dots represent the different voltages (red: 12 kV, orange: 11 kV, green: 10 kV, blue: 9 kV and purple: 8 kV)

From the slope of t_D vs $1/V$ for a given ion, we determined the ion mobility value K , from which we deduced the reduced ion mobility K_0 and its ${}^{\text{DT}}\text{CCS}(\text{N}_2)$ using the Mason-Schamp equation. Figure 3(B) shows the plot t_D vs $1/V$ resulting from the drift time of the same ion $[\text{PW}_{12}\text{O}_{40} +$

$\text{TBA}]^{2-}$ (m/z 1559) as Figure 3(A). We have determined for this ion a mobility value K of $1.303 \cdot 10^{-4} \text{ m}^2 \cdot \text{V}^{-1} \cdot \text{s}^{-1}$ at 30.7°C .

${}^{\text{DT}}\text{CCS}(\text{N}_2)$ values for the species $[\text{POM} + x\text{TBA} + y\text{H}]^{[n-(x+y)]-}$, where n is the POM naked charge, x the number of TBA counter ions and y the number of H^+ proton, in N_2 buffer gas are listed in table 1.

Expectedly, ion series showed a linear increase of around 45 \AA^2 when adding a TBA counter-ion within the POM cluster. This increase was observed at charge state 4^- , where we can see an increase of 46 \AA^2 between $[\text{P}_2\text{W}_{18}\text{O}_{62} + 2\text{H}]^{4-}$ (466 \AA^2) and $[\text{P}_2\text{W}_{18}\text{O}_{62} + \text{TBA} + \text{H}]^{4-}$ (512 \AA^2), and 43 \AA^2 between $[\text{P}_2\text{W}_{18}\text{O}_{62} + \text{TBA} + \text{H}]^{4-}$ (512 \AA^2) and $[\text{P}_2\text{W}_{18}\text{O}_{62} + 2\text{TBA}]^{4-}$ (555 \AA^2), and at charge state 3^- , where we can observe an increase of 40 \AA^2 between $[\text{P}_2\text{W}_{18}\text{O}_{62} + \text{TBA} + 2\text{H}]^{3-}$ (441 \AA^2) and $[\text{P}_2\text{W}_{18}\text{O}_{62} + 2\text{TBA} + \text{H}]^{3-}$ (483 \AA^2) and 42 \AA^2 between $[\text{P}_2\text{W}_{18}\text{O}_{62} + 2\text{TBA} + \text{H}]^{3-}$ (483 \AA^2) and $[\text{P}_2\text{W}_{18}\text{O}_{62} + 3\text{TBA}]^{3-}$ (523 \AA^2).

The value of approximately 40 to 45 \AA^2 for the TBA is very different from the value for TBA^+ alone which is 166 \AA^2 (${}^{\text{DT}}\text{CCS}(\text{N}_2)$).⁴¹ This was expected as, geometrically, the CCS of adducts are lower than the sum of its parts, and here, the charge state of the cluster may play a significant role as well.

Surprisingly, the CCS of several ions with different charge states showed very low CCS difference despite the addition of a TBA counter ion, for example $[\text{PW}_{12}\text{O}_{40}]^{3-}$ (340 \AA^2) and $[\text{PW}_{12}\text{O}_{40} + \text{TBA}]^{2-}$ (350 \AA^2), and $[\text{PMo}_{12}\text{O}_{40}]^{3-}$ (349 \AA^2) and $[\text{PMo}_{12}\text{O}_{40} + \text{TBA}]^{2-}$ (351 \AA^2). Also, the CCS decreased between $[\text{W}_{10}\text{O}_{32} + \text{TBA}]^{3-}$ (395 \AA^2) and $[\text{W}_{10}\text{O}_{32} + \text{TBA} + \text{H}]^{2-}$ (329 \AA^2) despite having the same number of TBA counter ions in the cluster. Structural differences and the location of the TBA could also account for deviations in the trends depending on cluster size.

In addition, we observed a lower CCS at 60°C compared to 30°C for all ions (3% on average), which can be explained by a greater average speed of the gas molecules in the drift cell¹⁴.

DTIMS CCS comparison

The ${}^{\text{DT}}\text{CCS}(\text{N}_2)$ at 30°C of the POM ions in this study were linearly correlated to the ${}^{\text{DT}}\text{CCS}(\text{He})$ from the study from Surman *et al.*,³⁵ with a determination coefficient R^2 of 0.87 (Figure S19). A notable exception was $[\text{P}_2\text{W}_{18}\text{O}_{62} + \text{H}]^{5-}$ (m/z 873) which lied well outside this correlation (${}^{\text{DT}}\text{CCS}(\text{N}_2) : 568 \text{ \AA}^2$ and ${}^{\text{DT}}\text{CCS}(\text{He}) : 209 \text{ \AA}^2$). This calls again into question the presence of H^+ proton in an aprotic and polar solvent as acetonitrile. These protonated ions are expected to be formed either from residual water in the instrument or from fragmentation of the TBA adducts. Their formation process may be instrument dependent and affect the measured CCS if fragmentation or addition processes occur in the ion mobility device.

TWIMS CCS calibration

For the TWIMS calibrations, we used ${}^{\text{DT}}\text{CCS}$ values either in He (polyalanine²⁸ and dextran³⁰ or oligothymidine dT_{10} ¹⁷ or POM anions³⁵) or in N_2 (polyalanine²⁸ and dextran³⁰ or POM anions). The calibration curves obtained (Figure 4a) with the ${}^{\text{DT}}\text{CCS}(\text{He})$ of polyalanine and dextran or dT_{10} both showed determination coefficients R^2 higher than 0.998, and similar

slopes (0.68 and 0.67) but a notable shift in the intercept (that corresponds to the multiplying factor in the power function) between singly- and multiply-charged ions, as has been observed before by Gelb *et al.*⁴² The calibration line obtained from the ^{DT}CCS(He) values of nine standards POM measured by Surman *et al.*³⁵ covered a wider range of reduced CCS (Ω') and drift times. However, the correlation, under our analysis conditions, led to a smaller determination coefficient R^2 of 0.974, and showed a significant difference in both slope (0.84) and intercept (4.63) with the other two previous curves using ^{DT}CCS(He). This may be due to the existence of more significant differences in the collision phenomena between helium and nitrogen for POM compared to polypeptides and oligonucleotides.⁴² Indeed, TWIMS measurements are carried out in N₂, which is much more polarizable than helium and the very polar metal-oxygen bonds in the POM are expected to interact differently with the two collision gas.^{43,44}

We have thus plotted the calibration curves from the ^{DT}CCS(N₂) values of the POM from Table 1 (Figure 4). Among the ^{DT}CCS(N₂), values at *m/z* 921 [P₂W₁₈O₆₂+TBA]⁵⁻ and *m/z* 1176 [W₁₀O₃₂+2H]²⁻ were excluded, because the ions did not appear in the TWIMS analysis. We also did not use values at *m/z* 784 [W₁₀O₃₂+H]³⁻, *m/z* 872 [P₂W₁₈O₆₂+H]⁵⁻ and *m/z* 1151 [P₂W₁₈O₆₂+TBA+H]⁴⁻, which degraded the quality of the correlation. Note that the value at *m/z* 872 was excluded when comparing ^{DT}CCS(He) and ^{DT}CCS(N₂). These ions are all protonated and their CCS may be instrument dependent. Finally, ions from the TBA₉P₂Nb₃W₁₅O₆₂ POM were not used because we used them to validate TWIMS CCS from the POM calibration in the last part of this study.

The two curves lines obtained from the fourteen POM ^{DT}CCS(N₂) values, and from polyalanine and dextran ^{DT}CCS(N₂) values present similar trendlines, with a linear determination coefficient of 0.997 for the polyalanine and dextran calibration and 0.995 for the POM calibration (Figure 4b). The calibration curves of POM and polyalanine and dextran are also much more similar in nitrogen than in helium, with respective slopes of 0.49 and 0.53. As in helium, we observed a slight shift of the intercept between singly charged and multiply-charged reference ions (5.84 and 5.70, respectively, in nitrogen). It should be noted that the POM calibration from the 14 values of ^{DT}CCS(N₂) covered a wider range of reduced CCS (Ω') and drift times than polyalanine and dextran, in particular toward low drift times and Ω' values. A correlation was also tested using the ^{DT}CCS(N₂) values measured at 59.9°C (Figure S20) : the determination coefficient was as high (0.998), the slope was similar and only the value of the intercept changed (5.80).

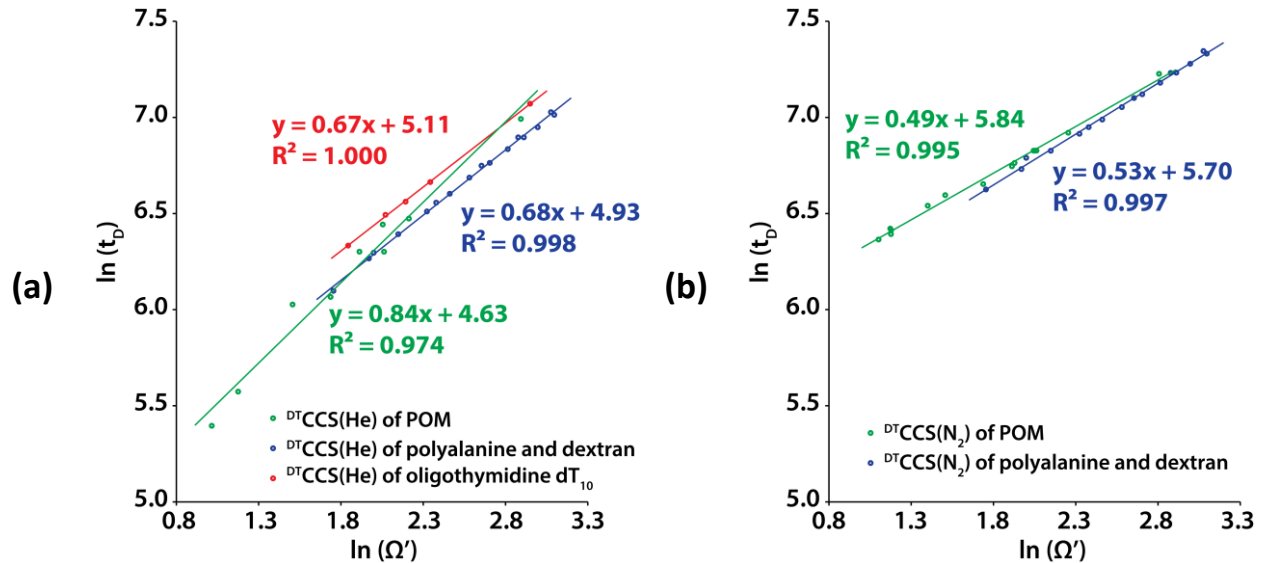


Figure 4 : Comparison of traveling wave drift time and reduced cross section Ω' from (a) ${}^{\text{DT}}\text{CCS}(\text{He})$ POM ions³⁵ (green), polyalanine/dextran^{28,30} (blue circle) and oligothymidine dT_{10} ¹⁷ (red circle) from the literature (B) ${}^{\text{DT}}\text{CCS}(N_2)$ of POM ions (green) from our measurements and reference ${}^{\text{DT}}\text{CCS}(N_2)$ of polyalanine and dextran^{28,30} (blue).

TWIMS CCS measurement and accuracy

In order to verify the calibration of the TWIMS cell, we used six POM ions from the Dawson structures $\text{TBA}_9\text{P}_2\text{Nb}_3\text{W}_{15}\text{O}_{62}$ with measured ${}^{\text{DT}}\text{CCS}(N_2)$, and we calculated their ${}^{\text{TW}}\text{CCS}_{(\text{N}2 \rightarrow \text{N}2)}$ with POM calibration and polyalanine and dextran calibration, in order to compare to ${}^{\text{DT}}\text{CCS}(N_2)$ (Table 2). All the chosen ions fit perfectly into the POM calibration range, while four of the ions were out of the calibration range with polyalanine and dextran (Table 2 and Figure S20). In spite of this, and using the equation of the calibration lines, the ${}^{\text{TW}}\text{CCS}_{(\text{N}2 \rightarrow \text{N}2)}$ of the $\text{P}_2\text{Nb}_3\text{W}_{15}\text{O}_{62}$ derived ions were determined and compared to the absolute values of ${}^{\text{DT}}\text{CCS}(N_2)$ (Table 2).

The relative error obtained with the polyalanine and dextran calibration was between -4.1% to -10.1% (average-7.5%) for the $\text{TBA}_9\text{P}_2\text{Nb}_3\text{W}_{15}\text{O}_{62}$ ions with the highest relative errors for $\text{TBA}_9\text{P}_2\text{Nb}_3\text{W}_{15}\text{O}_{62}$ ions with a charge state of 4-; notably all CCS were underestimated, suggesting a systematic bias when calibrating with a different compound class as already reported previously⁴⁵. The relative error obtained with the POM calibration is between -3.0% and 0.6% (average 2 %). Small relative errors obtained with the POM calibration are not surprising, and can be explained on the one hand by the fact that the ${}^{\text{DT}}\text{CCS}(\text{N}_2)$ of the $\text{P}_2\text{Nb}_3\text{W}_{15}\text{O}_{62}$ derived ions and the standards POM were determined on the same device. Furthermore, POM calibration is performed with multiply-charged ions unlike calibration with singly-charged ions of polyalanine and dextran.

Conclusion

We herein present a novel calibration strategy for determination of CCS values for multiply negatively charged ions on TWIM-MS devices (${}^{\text{TW}}\text{CCS}(\text{N}_2 \rightarrow \text{N}_2)$). The approach is based on the measurement of references CCS values using DTIMS in nitrogen (${}^{\text{DT}}\text{CCS}(\text{N}_2)$) for multiple POM structures. The calibration with POMs covers a wider range of CCS and drift times compared to commonly used polyalanine and dextran. Additionally, accuracy is greatly improved as demonstrated for six ions derived from Dawson-structured $\text{P}_2\text{Nb}_3\text{W}_{15}\text{O}_{62}$: whereas the average error in CCS determination using polyalanine and dextran calibration is 7.5%, it is only 2% using the POM calibration. The results demonstrate that accurate determination of CCS using TWIM-MS is possible for metal complexes using a compound-matched calibration routine. We believe that our approach can be applied to CCS determination of anionic metal-based coordination compounds by TWIM-MS in general and could therefore greatly aid in structural analysis of this compound class.

Acknowledgments

The authors gratefully acknowledge the Région Normandie, the Labex SynOrg (ANR-11-LABX-0029) and the European Regional Development Fund (ERDF 31708) for financial support.

References

1. Katsoulis DE. A Survey of Applications of Polyoxometalates. *Chem. Rev.* 1998;98(1):359–388. doi:10.1021/cr960398a.
2. Cronin L, Müller A. From serendipity to design of polyoxometalates at the nanoscale, aesthetic beauty and applications. *Chem. Soc. Rev.* 2012;41(22):7333. doi:10.1039/c2cs90087d.
3. Pope M., Jeannin Y, Fournier M. *Heteropoly and Isopoly Oxometalates*. Springer Berlin, Berlin, 2013.
4. Lau T-C, Wang J, Guevremont R, Siu KWM. Electrospray tandem mass spectrometry of polyoxoanions. *J. Chem. Soc. Chem. Commun.* 1995;(8):877. doi:10.1039/c39950000877.
5. Dablemont C, Proust A, Thouvenot R, Afonso C, Fournier F, Tabet J-C. Functionalization of Polyoxometalates: From Lindqvist to Keggin Derivatives. 1. Synthesis, Solution Studies, and

- Spectroscopic and ESI Mass Spectrometry Characterization of the Rhenium Phenylimido Tungstophosphate [PW₁₁O₃₉{ReNC₆H₅}]⁴⁻. *Inorg. Chem.* 2004;43(11):3514–3520. doi:10.1021/ic0499042.
- 6. Mayer CR, Roch-Marchal C, Lavanant H, Thouvenot R, Sellier N, Blais J-C, Sécheresse F. New Organosilyl Derivatives of the Dawson Polyoxometalate [α₂-P₂W₁₇O₆₁(RSi)₂O]⁶⁻: Synthesis and Mass Spectrometric Investigation. *Chem. - Eur. J.* 2004;10(21):5517–5523. doi:10.1002/chem.200400217.
 - 7. Piot M, Hupin S, Lavanant H, Afonso C, Bouteiller L, Proust A, Izet G. Charge Effect on the Formation of Polyoxometalate-Based Supramolecular Polygons Driven by Metal Coordination. *Inorg. Chem.* 2017;56(14):8490–8496. doi:10.1021/acs.inorgchem.7b01187.
 - 8. Song Y-F, Long D-L, Kelly SE, Cronin L. Sorting the Assemblies of Unsymmetrically Covalently Functionalized Mn-Anderson Polyoxometalate Clusters with Mass Spectrometry. *Inorg. Chem.* 2008;47(20):9137–9139. doi:10.1021/ic801366r.
 - 9. Miras HN, Wilson EF, Cronin L. Unravelling the complexities of inorganic and supramolecular self-assembly in solution with electrospray and cryospray mass spectrometry. *Chem. Commun.* 2009;(11):1297. doi:10.1039/b819534j.
 - 10. Kanu AB, Dwivedi P, Tam M, Matz L, Hill HH. Ion mobility-mass spectrometry. *J. Mass Spectrom.* 2008;43(1):1–22. doi:10.1002/jms.1383.
 - 11. Lanucara F, Holman SW, Gray CJ, Evers CE. The power of ion mobility-mass spectrometry for structural characterization and the study of conformational dynamics. *Nat. Chem.* 2014;6(4):281–294. doi:10.1038/nchem.1889.
 - 12. Mason EA, McDaniel EW. *Transport Properties of Ions in Gases*. Wiley-VCH Verlag GmbH & Co. KGaA, Weinheim, FRG, 1988.
 - 13. Mosier PD, Counterman AE, Jurs PC, Clemmer DE. Prediction of Peptide Ion Collision Cross Sections from Topological Molecular Structure and Amino Acid Parameters. *Anal. Chem.* 2002;74(6):1360–1370. doi:10.1021/ac0112059.
 - 14. Revercomb HE, Mason EA. Theory of plasma chromatography/gaseous electrophoresis. Review. *Anal. Chem.* 1975;47(7):970–983. doi:10.1021/ac60357a043.
 - 15. Clemmer DE, Jarrold MF. Ion Mobility Measurements and their Applications to Clusters and Biomolecules. *J. Mass Spectrom.* 1997;32(6):577–592. doi:10.1002/(SICI)1096-9888(199706)32:6<577::AID-JMS530>3.0.CO;2-4.
 - 16. Counterman AE, Valentine SJ, Srebalus CA, Henderson SC, Hoaglund CS, Clemmer DE. High-order structure and dissociation of gaseous peptide aggregates that are hidden in mass spectra. *J. Am. Soc. Mass Spectrom.* 1998;9(8):743–759. doi:10.1016/S1044-0305(98)00052-X.
 - 17. Hoaglund CS, Liu Y, Ellington AD, Pagel M, Clemmer DE. Gas-Phase DNA: Oligothymidine Ion Conformers. *J. Am. Chem. Soc.* 1997;119(38):9051–9052. doi:10.1021/ja970652w.
 - 18. Henderson SC, Valentine SJ, Counterman AE, Clemmer DE. ESI/Ion Trap/Ion Mobility/Time-of-Flight Mass Spectrometry for Rapid and Sensitive Analysis of Biomolecular Mixtures. *Anal. Chem.* 1999;71(2):291–301. doi:10.1021/ac9809175.
 - 19. Wyttenbach T, von Helden G, Bowers MT. Gas-Phase Conformation of Biological Molecules: Bradykinin. *J. Am. Chem. Soc.* 1996;118(35):8355–8364. doi:10.1021/ja9535928.
 - 20. Valentine SJ, Counterman AE, Clemmer DE. Conformer-dependent proton-transfer reactions of ubiquitin ions. *J. Am. Soc. Mass Spectrom.* 1997;8(9):954–961. doi:10.1016/S1044-0305(97)00085-8.
 - 21. Shelimov KB, Clemmer DE, Hudgins RR, Jarrold MF. Protein Structure *in Vacuo* : Gas-Phase Conformations of BPTI and Cytochrome c. *J. Am. Chem. Soc.* 1997;119(9):2240–2248. doi:10.1021/ja9619059.
 - 22. Valentine SJ, Anderson JG, Ellington AD, Clemmer DE. Disulfide-Intact and -Reduced Lysozyme in the Gas Phase: Conformations and Pathways of Folding and Unfolding. *J. Phys. Chem. B* 1997;101(19):3891–3900. doi:10.1021/jp970217o.

23. Bush MF, Hall Z, Giles K, Hoyes J, Robinson CV, Ruotolo BT. Collision Cross Sections of Proteins and Their Complexes: A Calibration Framework and Database for Gas-Phase Structural Biology. *Anal. Chem.* 2010;82(22):9557–9565. doi:10.1021/ac1022953.
24. Bush MF, Campuzano IDG, Robinson CV. Ion Mobility Mass Spectrometry of Peptide Ions: Effects of Drift Gas and Calibration Strategies. *Anal. Chem.* 2012;84(16):7124–7130. doi:10.1021/ac3014498.
25. Salbo R, Bush MF, Naver H, Campuzano I, Robinson CV, Pettersson I, Jørgensen TJD, Haselmann KF. Traveling-wave ion mobility mass spectrometry of protein complexes: accurate calibrated collision cross-sections of human insulin oligomers: Traveling-wave IM-MS of protein complexes. *Rapid Commun. Mass Spectrom.* 2012;26(10):1181–1193. doi:10.1002/rcm.6211.
26. Campuzano I, Bush MF, Robinson CV, Beaumont C, Richardson K, Kim H, Kim HI. Structural Characterization of Drug-like Compounds by Ion Mobility Mass Spectrometry: Comparison of Theoretical and Experimentally Derived Nitrogen Collision Cross Sections. *Anal. Chem.* 2012;84(2):1026–1033. doi:10.1021/ac202625t.
27. Fenn LS, Kliman M, Mahsut A, Zhao SR, McLean JA. Characterizing ion mobility-mass spectrometry conformation space for the analysis of complex biological samples. *Anal. Bioanal. Chem.* 2009;394(1):235–244. doi:10.1007/s00216-009-2666-3.
28. Forsythe JG, Petrov AS, Walker CA, Allen SJ, Pellissier JS, Bush MF, Hud NV, Fernández FM. Collision cross section calibrants for negative ion mode traveling wave ion mobility-mass spectrometry. *The Analyst* 2015;140(20):6853–6861. doi:10.1039/C5AN00946D.
29. Hamilton JV, Renaud JB, Mayer PM. Experiment and theory combine to produce a practical negative ion calibration set for collision cross-section determinations by travelling-wave ion-mobility mass spectrometry: Practical negative ion calibration set for collision cross-sections. *Rapid Commun. Mass Spectrom.* 2012;26(14):1591–1595. doi:10.1002/rcm.6266.
30. Hofmann J, Struwe WB, Scarff CA, Scrivens JH, Harvey DJ, Pagel K. Estimating Collision Cross Sections of Negatively Charged N-Glycans using Traveling Wave Ion Mobility-Mass Spectrometry. *Anal. Chem.* 2014;86(21):10789–10795. doi:10.1021/ac5028353.
31. Lavanant H, Tognetti V, Afonso C. Traveling Wave Ion Mobility Mass Spectrometry and Ab Initio Calculations of Phosphoric Acid Clusters. *J. Am. Soc. Mass Spectrom.* 2014;25(4):572–80. doi:10.1007/s13361-013-0818-3.
32. Smith DP, Knapman TW, Campuzano I, Malham RW, Berryman JT, Radford SE, Ashcroft AE. Deciphering Drift Time Measurements from Travelling Wave Ion Mobility Spectrometry-Mass Spectrometry Studies. *Eur. J. Mass Spectrom.* 2009;15(2):113–130. doi:10.1255/ejms.947.
33. Thiel J, Yang D, Rosnes MH, Liu X, Yvon C, Kelly SE, Song Y-F, Long D-L, Cronin L. Observing the Hierarchical Self-Assembly and Architectural Bistability of Hybrid Molecular Metal Oxides Using Ion-Mobility Mass Spectrometry. *Angew. Chem. Int. Ed.* 2011;50(38):8871–8875. doi:10.1002/anie.201102340.
34. Izett G, Macdonell A, Rinfray C, Piot M, Renaudineau S, Derat E, Abécassis B, Afonso C, Proust A. Metal-Directed Self-Assembly of a Polyoxometalate-Based Molecular Triangle: Using Powerful Analytical Tools to Probe the Chemical Structure of Complex Supramolecular Assemblies. *Chem. - Eur. J.* 2015;21(52):19010–19015. doi:10.1002/chem.201503363.
35. Surman AJ, Robbins PJ, Ujma J, Zheng Q, Barran PE, Cronin L. Sizing and Discovery of Nanosized Polyoxometalate Clusters by Mass Spectrometry. *J. Am. Chem. Soc.* 2016;138(11):3824–3830. doi:10.1021/jacs.6b00070.
36. Booth HS. *Inorganic Syntheses*. McGraw-Hill : [Then] J. Wiley And Sons, New York, 1939.
37. Rocchiccioli-Deltcheff C, Fournier M, Franck R, Thouvenot R. Vibrational investigations of polyoxometalates. 2. Evidence for anion-anion interactions in molybdenum(VI) and tungsten(VI) compounds related to the Keggin structure. *Inorg. Chem.* 1983;22(2):207–216. doi:10.1021/ic00144a006.
38. Long D-L, Streb C, Song Y-F, Mitchell S, Cronin L. Unravelling the Complexities of Polyoxometalates in Solution Using Mass Spectrometry: Protonation versus Heteroatom Inclusion. *J. Am. Chem. Soc.* 2008;130(6):1830–1832. doi:10.1021/ja075940z.

39. Weiner H, Aiken JD, Finke RG. Polyoxometalate Catalyst Precursors. Improved Synthesis, H⁺-Titration Procedure, and Evidence for ³¹P NMR as a Highly Sensitive Support-Site Indicator for the Prototype Polyoxoanion–Organometallic-Support System [(n-C₄H₉)₄N]₉P₂W₁₅Nb₃O₆₂. *Inorg. Chem.* 1996;35(26):7905–7913. doi:10.1021/ic960681s.
40. Kwasnik M, Fuhrer K, Gonin M, Barbeau K, Fernández FM. Performance, Resolving Power, and Radial Ion Distributions of a Prototype Nanoelectrospray Ionization Resistive Glass Atmospheric Pressure Ion Mobility Spectrometer. *Anal. Chem.* 2007;79(20):7782–7791. doi:10.1021/ac071226o.
41. Campuzano I, Bush MF, Robinson CV, Beaumont C, Richardson K, Kim H, Kim HI. Structural Characterization of Drug-like Compounds by Ion Mobility Mass Spectrometry: Comparison of Theoretical and Experimentally Derived Nitrogen Collision Cross Sections. *Anal. Chem.* 2012;84(2):1026–1033. doi:10.1021/ac202625t.
42. Gelb AS, Jarratt RE, Huang Y, Dodds ED. A Study of Calibrant Selection in Measurement of Carbohydrate and Peptide Ion-Neutral Collision Cross Sections by Traveling Wave Ion Mobility Spectrometry. *Anal. Chem.* 2014;86(22):11396–11402. doi:10.1021/ac503379e.
43. Beegle LW, Kanik I, Matz L, Hill HH. Effects of drift-gas polarizability on glycine peptides in ion mobility spectrometry. *Int. J. Mass Spectrom.* 2002;216(3):257–268. doi:10.1016/S1387-3806(02)00626-7.
44. Matz LM, Hill HH, Beegle LW, Kanik I. Investigation of drift gas selectivity in high resolution ion mobility spectrometry with mass spectrometry detection. *J. Am. Soc. Mass Spectrom.* 2002;13(4):300–307. doi:10.1016/S1044-0305(01)00366-X.
45. Hines KM, May JC, McLean JA, Xu L. Evaluation of Collision Cross Section Calibrants for Structural Analysis of Lipids by Traveling Wave Ion Mobility-Mass Spectrometry. *Anal. Chem.* 2016;88(14):7329–7336. doi:10.1021/acs.analchem.6b01728.

Supporting information

ESI mass spectra of the six POM compounds. Drift time vs 1/V plots of the twenty-six POM-derived anions at 30°C and 60°C. Correlation of ^{DT}CCS(N₂) vs TBA number for POM ions. Comparison ^{DT}CCS(N₂) vs ^{DT}CCS(He) for Keggin and Dawson ions. Table of the average of drift times and FWHM observed on the TWIMS cell of Synapt G2 of POM ions. Comparison of traveling wave drift time and reduced cross section Ω' from ^{DT}CCS(N₂) 60°C of POM ions (cyan) from our measurements and reference ^{DT}CCS(N₂) of polyalanine and dextran (blue). Comparison of drift time and reduced cross section Ω' of P₂Nb₃W₁₅O₆₂ derived anions with that POM (A) and polyalanine and dextran (B) references ions in nitrogen.

Table 1 : List of ion mobility K (in $\text{cm}^2 \cdot \text{V}^{-1} \cdot \text{s}^{-1}$) and CCS values (in \AA^2) obtained from the six standard POMs in nitrogen, at two different temperatures (30.7°C and 59.9°C) ; values in italics were not used in the calibration ; * $P_2\text{Nb}_3\text{W}_{15}\text{O}_{62}$ ions in bold italics were not used in the calibration but were used to estimate the relative error in CCS estimation resulting from the calibration. ${}^{DT}\text{CCS}(\text{He})$ from Surman et al are shown for comparison.

Compound	Structure	Ion observed	<i>m/z</i>	z	30.7°C		59.9°C		26.85°C	
					K_0 ($\text{cm}^2 \cdot \text{V}^{-1} \cdot \text{s}^{-1}$)	${}^{DT}\text{CCS}(\text{N}_2)$ (\AA^2)	K_0 ($\text{cm}^2 \cdot \text{V}^{-1} \cdot \text{s}^{-1}$)	${}^{DT}\text{CCS}(\text{N}_2)$ (\AA^2)	${}^{DT}\text{CCS}(\text{He})$ (\AA^2) ³⁵	
TBA ₂ Mo ₆ O ₁₉	Lindqvist	[Mo ₆ O ₁₉] ²⁻	439.79	2	1.85	223	1.80	220	-	
		[Mo ₆ O ₁₉ +TBA] ⁻	1122.04	1	0.77	263	0.76	254	-	
TBA ₄ W ₁₀ O ₃₂	Decatungstate	[W ₁₀ O ₃₂ +H] ³⁻	784.47	3	1.81	339	1.80	339	-	
		[W ₁₀ O ₃₂ +TBA] ³⁻	864.29	3	1.55	395	1.54	380	-	
		[W ₁₀ O ₃₂ +2H] ²⁻	1176.21	2	1.52	267	1.50	258	-	
		[W ₁₀ O ₃₂ +TBA+H] ²⁻	1296.94	2	1.23	329	1.21	321	-	
		[W ₁₀ O ₃₂ +2TBA] ²⁻	1417.66	2	1.06	384	1.03	377	-	
		[PMo ₁₂ O ₄₀] ³⁻	607.38	3	1.77	349	1.75	336	-	
TBA ₃ PMo ₁₂ O ₄₀	Keggin	[PMo ₁₂ O ₄₀ +TBA] ²⁻	1032.30	2	1.16	351	1.13	342	-	
TBA ₃ PW ₁₂ O ₄₀	Keggin	[PW ₁₂ O ₄₀] ³⁻	959.02	3	1.79	340	1.75	334	150	
		[PW ₁₂ O ₄₀ +TBA] ²⁻	1559.76	2	1.15	350	1.13	342	207	
TBA ₆ P ₂ W ₁₈ O ₆₂	Dawson	[P ₂ W ₁₈ O ₆₂ +H] ⁵⁻	872.81	5	1.79	568	1.80	541	209	
		[P ₂ W ₁₈ O ₆₂ +TBA] ⁵⁻	921.11	5	1.69	606	1.68	578	-	
		[P ₂ W ₁₈ O ₆₂ +2H] ⁴⁻	1091.27	4	1.75	466	1.74	446	-	
		[P ₂ W ₁₈ O ₆₂ +TBA+H] ⁴⁻	1151.63	4	1.59	512	1.59	491	-	
		[P ₂ W ₁₈ O ₆₂ +2TBA] ⁴⁻	1212.00	4	1.46	555	1.46	531	314	
		[P ₂ W ₁₈ O ₆₂ +TBA+2H] ³⁻	1535.85	3	1.38	441	1.35	429	245	
		[P ₂ W ₁₈ O ₆₂ +2TBA+H] ³⁻	1616.33	3	1.26	483	1.23	472	310	
		[P ₂ W ₁₈ O ₆₂ +3TBA] ³⁻	1696.82	3	1.16	523	1.14	508	357	
TBA ₉ P ₂ Nb ₃ W ₁₅ O ₆₂ *	Dawson	[P ₂ Nb ₃ W ₁₅ O ₆₂ +5H] ⁴⁻	1023.83	4	1.72	473	-	-	-	
		[P ₂ Nb ₃ W ₁₅ O ₆₂ +TBA+4H] ⁴⁻	1084.19	4	1.57	518	-	-	-	
		[P ₂ Nb ₃ W ₁₅ O ₆₂ +2TBA+3H] ⁴⁻	1144.55	4	1.46	557	-	-	-	
		[P ₂ Nb ₃ W ₁₅ O ₆₂ +3TBA+2H] ⁴⁻	1204.92	4	1.37	595	-	-	-	
		[P ₂ Nb ₃ W ₁₅ O ₆₂ +TBA+5H] ³⁻	1445.92	3	1.38	443	-	-	-	
		[P ₂ Nb ₃ W ₁₅ O ₆₂ +2TBA+4H] ³⁻	1526.41	3	1.25	486	-	-	-	
		[P ₂ Nb ₃ W ₁₅ O ₆₂ +3TBA+3H] ³⁻	1606.89	3	1.15	526	-	-	-	

Table 2 : $^{DT}CCS(N_2)$ values of $TBA_9P_2Nb_3W_{15}O_{62}$ ions, and $^{TW}CCS(N_2 \rightarrow N_2)$ obtained from POM calibration and polyalanine and dextran monocharged calibration. Relative error between $^{DT}CCS(N_2)$ values and the two TWIMS calibration is also calculated. Bold values correspond to $TBA_9P_2Nb_3W_{15}O_{62}$ ions that are out of calibration range with polyalanine and dextran.

Ion observed	m/z	z	$^{DT}CCS(N_2)$	$^{TW}CCS(N_2 \rightarrow N_2)$			$^{TW}CCS(N_2 \rightarrow N_2)$ with polyalanine and dextran calibration (\AA^2)	Relative error (%)	Relative error (%)
			(\AA^2)	with POM calibration (\AA^2)	Relative error (%)				
$[P_2Nb_3W_{15}O_{62}+TBA+4H]^{4-}$	1084.19	-4	518	508	-1.9	467	-9.8		
$[P_2Nb_3W_{15}O_{62}+2TBA+3H]^{4-}$	1144.55	-4	557	542	-2.7	501	-10.1		
$[P_2Nb_3W_{15}O_{62}+3TBA+2H]^{4-}$	1204.92	-4	595	577	-3.0	537	-9.7		
$[P_2Nb_3W_{15}O_{62}+TBA+5H]^{3-}$	1445.92	-3	443	455	2.7	425	-4.1		
$[P_2Nb_3W_{15}O_{62}+2TBA+4H]^{3-}$	1526.41	-3	486	494	1.6	466	-4.1		
$[P_2Nb_3W_{15}O_{62}+3TBA+3H]^{3-}$	1606.89	-3	526	529	0.6	502	-4.6		